Available online at www.sciencedirect.com
ScienceDirect
Journal of Sound and Vibration 322 (2009) 756–771
JOURNAL OF SOUND AND VIBRATION
www.elsevier.com/locate/jsvi

System identification of an enclosure with leakages using a probabilistic approach

H.F. Lam[a], C.T. Ng[b,*], Y.Y. Lee[a], H.Y. Sun[a]

[a]*Department of Building and Construction, City University of Hong Kong, 83 Tat Chee Avenue, Kowloon, Hong Kong*
[b]*School of Engineering, The University of Queensland, Brisbane, Australia*

Received 19 September 2007; received in revised form 18 August 2008; accepted 9 November 2008
Handling Editor: L.G. Tham
Available online 24 December 2008

Abstract

This paper presents a model-based method for the system identification of a rectangular enclosure with an unknown number of air leakages subjected to uniform external noise, according to the probabilistic approach. The method aims to identify the number and corresponding locations and sizes of air leakages utilizing a set of measured, interior, sound pressure data in the frequency domain.

System identification of an enclosure with an unknown number of air leakages is not trivial. Different classes of acoustic models are required to simulate an enclosure with different numbers of leakages. By following the traditional system of identification techniques, the ''optimal'' class of models is selected by minimizing the discrepancy between the measured and modeled interior sound pressure. By doing this, the most complicated model class (that is, the one with the highest number of uncertain parameters) will always be selected. Therefore, the traditional system identification techniques found in the literature to date cannot be employed to solve this problem.

Our proposed system identification methodology relies on the Bayesian information criterion (BIC) to identify accurately the number of leakages in an enclosure. Unlike all deterministic system identification approaches, the proposed methodology aims to calculate the posterior (updated) probability density function (PDF) of leakage locations and sizes. Therefore, the uncertainties introduced by measurement noise and modeling error can be explicitly addressed. The coefficient of variable (COV) of uncertain parameters, which can be easily calculated from the PDF, provides valuable information about the reliability of the identification results.

1. Introduction

The modeling of an acoustic enclosure is an important issue, and many researchers [1–5] have developed different theoretical methods to address this problem. Oldham and Hillarby [4,6] and Pan et al. [5] carried out both theoretical and experimental studies of the modeling of acoustic enclosures. In their findings, they reported that some assigned model parameters were not accurate due to the uncertainties associated with the boundary conditions, material properties and damping of the system. System identification allows researchers

*Corresponding author. Tel.: +61 7 3365 3536.
E-mail address: c.ng2@uq.edu.au (C.T. Ng).

0022-460X/$ - see front matter © 2008 Elsevier Ltd. All rights reserved.
doi:10.1016/j.jsv.2008.11.013

and engineers to increase the accuracy of model parameters and to obtain a representative model, which can then be employed for predictions and controls. McKelvey et al. [7] proposed a subspace system identification method to identify the acoustic model of a regular duct using frequency response data. Henry and Clark [8] set up the transfer functions for particular inputs and outputs of an acoustic model, which was then used in the design of a control system based on system identification. Fang et al. [9] presented a paper on the modeling, system identification and control of acoustic-structure interaction dynamics of enclosure systems. The transfer function and state-space models were obtained from experimental data using system identification techniques. The identified model was then used for controller design. Lee et al. [10] proposed a probabilistic approach to identify the uncertain parameters of the acoustic model of a room utilizing the measured interior sound pressure. The identified acoustic model was then used to reconstruct the interior sound pressure distribution. Lardies [11] utilized the wavelet transform of free responses for the identification of eigen frequencies of damped signals. The method has been demonstrated using numerical and experimental results from an acoustic enclosure.

The main objective of this paper is to develop a probabilistic method for the system identification of an enclosure with an unknown number of leakages, utilizing measured interior sound pressure introduced by uniform external noise. There are many system identification methods in the existing literature. The basic idea of most of them is to minimize the discrepancy between the measured and calculated, or predicted, model outputs. It must be pointed out that the idea of minimizing the discrepancy is not applicable in the system identification of enclosures with an unknown number of leakages. This is because different classes of models are needed to represent enclosures with different numbers of leakages. The model class of an enclosure with more leakages consists of more model parameters, and therefore, is more complex than the model class of an enclosure with fewer leakages. As a more complex model class can always better accommodate the measured interior sound pressure than a less complex one, the most complex model class will always be selected when following this approach. To overcome this difficulty, our proposed methodology relies on the Bayesian information criterion (BIC) by identifying the "optimal" model class for a given set of measured interior sound pressures, with the objective of determining the number of air leakages.

The proposed system identification methodology not only identifies the model parameters, but also the associated uncertainties. This can be achieved by calculating the posterior (updated) probability density function (PDF) of the leakage locations and their corresponding sizes. With the calculated PDF, the coefficient of variation (COV) of the identified parameters can be easily calculated. The COV provides valuable information on the reliability of the system identification results. This information cannot be obtained by any deterministic system identification methods.

A series of comprehensive case studies were carried out to verify and demonstrate the proposed methodology. The results are very encouraging. By using our proposed methodology, we studied the effects of measurement noise, modeling error, the number of leakages and the number of measurement stations on the results of system identification through numerical simulation.

2. Proposed methodology

The proposed methodology is directed at the system identification of a rectangular enclosure with an unknown number of square leakages, as shown in Fig. 1, in which L_x, L_y and L_z are the dimensions of the enclosure, and N_l is the number of leakages. By assuming that all leakages are square and on the side wall, with $x = L_x$ (see Fig. 1), each leakage can be represented by three model parameters (that is, the y- and z-coordinates of the lower left corner of the leakage, and its size).

The basic strategy of the proposed methodology is to adopt different classes of acoustic models to represent a rectangular enclosure with different numbers of leakages. The identification of the number of leakages is then equivalent to the selection of the "optimal" class of models for a given set of measured interior sound pressure. It must be pointed out that a model class with more model parameters can better accommodate the measurement when compared to a model class with fewer model parameters. In the presence of measurement noise, the optimal model in the model class, say M_3, can fit the measurement better than that in M_2, as the three additional parameters can compensate for the effect of measurement noise to some extent. The selection of the "optimal" model class, based solely on the fit between the modeled and the measured interior sound

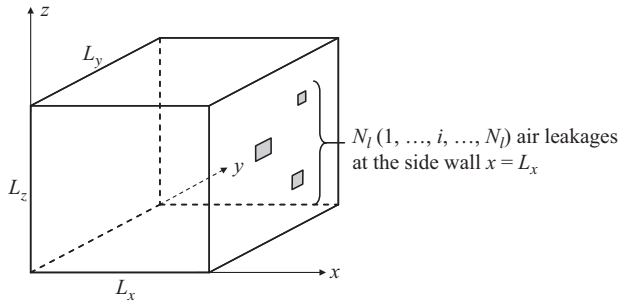

Fig. 1. The rectangular enclosure acoustic model with different number of air leakages.

pressure, is very misleading, as the most complex model class will always be selected. Our proposed methodology uses the probabilistic approach to address this problem. By following the Bayesian statistical framework [12], the conditional probability of a model class for a given set of data D can be approximated asymptotically. Under the assumption of a large number of measured data points, this probability can be further simplified as the BIC [13]. The formulation of the BIC for a class of models is presented in Section 2.2.

To quantify the uncertainties associated with the identification results, the posterior PDF of the set of uncertain model parameters (e.g., leakage locations and sizes) are calculated by again employing the Bayesian statistical framework [12], which is briefly reviewed in Section 2.3. The modeling of the rectangular enclosure with a given number of leakages is first given in the following section.

2.1. Modeling of an enclosure with leakages

A rectangular enclosure is shown in Fig. 1. The dimensions of the enclosure are $L_x \times L_y \times L_z$. It is assumed that the enclosure is subject to a steady-state uniform distributed sound pressure. The complex acoustic pressure $f(\mathbf{r})$ in the enclosure can be described by the frequency domain acoustic wave equation [5]

$$(\nabla^2 + \bar{k}^2) f(\mathbf{r}) = -\mathrm{j}\rho_0 \omega q(\mathbf{r}), \tag{1}$$

where $\bar{k} = \omega/c$ is the wavenumber; c is the sound speed; ρ_0 is the air density; ω is the angular frequency of the sound waves; $\mathbf{r}$ is the position vector; and $q(\mathbf{r})$ is the strength of the sound source describing the volume velocity per unit volume.

Based on the model expansion approach [5], the acoustic pressure field can be described by a trial solution $f^{(N_f)}(\mathbf{r})$, and the residual of Eq. (1) is defined as

$$R(f^{(N_f)}(\mathbf{r})) = (\nabla^2 + \bar{k}^2) f^{(N_f)}(\mathbf{r}) + \mathrm{j}\rho_0 \omega q(\mathbf{r}). \tag{2}$$

The trial solution $f^{(N_f)}(\mathbf{r})$ is assumed to be

$$f^{(N_f)}(\mathbf{r}) = \sum_{J=1}^{N_f} F_J \phi_J(\mathbf{r}), \tag{3}$$

where N_f are the number of acoustic modes considered; F_J is the pressure amplitude of the J-th acoustic mode; $\phi_J(\mathbf{r})$ are the shape functions that satisfy the geometrical boundary conditions of the sound field and are all orthogonal to the residual, that is, $\int_V \phi_J(\mathbf{r}) R(f^{(N_f)}(r))\,\mathrm{d}V = 0$. The following equation can be thus derived for each $\phi_J(\mathbf{r})$:

$$\int_V \phi_J(\mathbf{r}) \nabla^2 f^{(N_f)}(\mathbf{r})\,\mathrm{d}V + \bar{k}^2 \int_V \phi_J(\mathbf{r}) f^{(N_f)}(\mathbf{r})\,\mathrm{d}V = -\mathrm{j}\rho_0 \omega \int_V q(\mathbf{r}) \phi_J(\mathbf{r})\,\mathrm{d}V. \tag{4}$$

The first term on the left-hand side of Eq. (4) can be expressed as

$$\int_V \phi_J(\mathbf{r}) \nabla^2 f^{(N_f)}(\mathbf{r})\,\mathrm{d}V = \int_V f^{(N_f)}(\mathbf{r}) \nabla^2 \phi_J(\mathbf{r})\,\mathrm{d}V + \int_S \frac{\partial f^{(N_f)}(\mathbf{r})}{\partial n} \phi_J(\mathbf{r})\,\mathrm{d}S - \int_S \frac{\partial \phi_J(\mathbf{r})}{\partial n} f^{(N_f)}\mathrm{d}S. \tag{5}$$

Assuming the rectangular enclosures are constructed by rigid walls, the shape functions are

$$\phi_J(\mathbf{r}) = \phi_{lmn}(\mathbf{r}) = \cos\frac{l\pi x}{L_x}\cos\frac{m\pi y}{L_y}\cos\frac{n\pi z}{L_z}, \tag{6}$$

and the boundary conditions are

$$\left.\frac{\partial\phi}{\partial x}\right|_{x=0} = 0, \quad \left.\frac{\partial\phi}{\partial x}\right|_{x=L_x} = v(y,z), \quad \left.\frac{\partial\phi}{\partial y}\right|_{y=0} = \left.\frac{\partial\phi}{\partial y}\right|_{y=L_y} = 0, \quad \left.\frac{\partial\phi}{\partial z}\right|_{z=0} = \left.\frac{\partial\phi}{\partial z}\right|_{z=L_z} = 0. \tag{7}$$

where l, m and n are integers

Using Eqs. (4) and (5), the generalized coordinates F_J are

$$(\bar{k}^2 - \mathrm{j}\zeta\bar{k}\bar{k}_J - \bar{k}_J^2)\Lambda_J F_J = -\int_S \phi_J \frac{\partial f^{(N_f)}(\mathbf{r})}{\partial n}\mathrm{d}S - \mathrm{j}\rho_0\omega\int_V \phi_J q(\mathbf{r})\,\mathrm{d}V \tag{8}$$

for $J = 1, 2, \ldots, N_f$, where ζ is the damping ratio; $\Lambda_J = \int_V \phi_J^2(\mathbf{r})\,\mathrm{d}V$; and the second term of the right-hand side is related to the point sound source within the enclosure. In Fig. 1, it is assumed that N_l ($l = 1, \ldots, i, \ldots N_l$) air leakages are located at $x_i = L_x$, $y_i \leqslant y \leqslant y_i + L'_{y_i}$ and $z_i \leqslant z \leqslant z_i + L'_{z_i}$. L'_{y_i} and L'_{z_i} are the width and length of the i-th air leakage. The first term of the right-hand side in Eq. (8) represents the contribution from non-rigid boundary conditions, and it can be expressed as

$$\frac{\partial f^{(N_f)}(\mathbf{r})}{\partial n} = -\mathrm{j}\rho_0\omega v(y,z). \tag{9}$$

$\bar{k}_J$ is the wavenumber of the J-th rigid mode, and it is

$$\bar{k}_J = \bar{k}_{lmn} = \pi\sqrt{\left(\frac{l}{L_x}\right)^2 + \left(\frac{m}{L_y}\right)^2 + \left(\frac{n}{L_z}\right)^2}. \tag{10}$$

The velocity profiles at the air leakages are assumed to be double sine function as follows.

$$v(y,z) = \begin{cases} \mathrm{j}\omega B_i \sin\left(\dfrac{\pi(y-y_i)}{L'_{y_1}}\right)\sin\left(\dfrac{\pi(z-z_i)}{L'_{z_1}}\right) & \text{for the } i\text{-th air leakage} \\ 0 & \text{for the rigid wall} \end{cases}, \tag{11}$$

where B_i are the air particle displacement amplitudes at the i-th air leakage. Thus, Eq. (9) becomes

$$\int_S \phi_J \frac{\partial f^{(N_f)}(\mathbf{r})}{\partial n}\,\mathrm{d}S = \rho_0\omega^2 \sum_{i=1}^{N_l} B_i\alpha_{iJ}, \tag{12}$$

where α_{iJ} are the modal coupling coefficients of the J-th acoustic mode, which depends on the location and size of the i-th air leakage, as given below.

$$\alpha_{iJ} = \int_{S_i} \phi_J(\mathbf{r}) \sin\left(\frac{\pi(y-y_i)}{L'_{y_i}}\right)\sin\left(\frac{\pi(z-z_i)}{L'_{z_i}}\right)\mathrm{d}S, \tag{13}$$

where $S_i = L'_{y_i}L'_{z_i}$ are the i-th leakage area.

The displacement equation of movement at the i-th air leakage in the frequency domain is

$$-m\omega^2\bar{w}_i + \mathrm{j}\omega Q_i\bar{w}_i = \bar{f}_i - f_e, \tag{14}$$

where $m = \rho_0 h$ are the equivalent air mass at the leakages; h is the wall thickness; $Q_i = \rho_0 c\bar{k}^2 S_i/2\pi$ is the equivalent sound radiation impedance at the leakages [14]; $\bar{w}_i$ is the average air particle displacement; $\bar{f}_i$ and f_e are the interior sound pressure at the i-th air leakage and external sound pressure acting on the air piston, respectively. They are given as

$$\bar{w}_i = \frac{\int_{S_i} w(y,z)\,\mathrm{d}S}{S_i} = \frac{B_i\int_{S_i}\sin(\pi(y-y_i)/L'_{y_i})\sin(\pi(z-z_i)/L'_{z_i})\,\mathrm{d}S}{S_i} = B_i\left(\frac{2}{\pi}\right)^2 \tag{15}$$

and

$$\bar{f}_i = \frac{\int_{S_i} \sum_{I=1}^{N_f} F_I \phi_I(\mathbf{r})\,\mathrm{d}S}{S_i} = \sum_{I=1}^{N_f} F_I \beta_{iI}, \tag{16}$$

where β_{iI} are the coefficients in terms of the velocity mode of the air piston and given as

$$\beta_{iI} = \frac{\int_{S_i} \phi_I(\mathbf{r})\,\mathrm{d}S}{S_i}. \tag{17}$$

By using Eqs. (12), (14), (15) and (16); and then substituting the resulting equations into Eq. (8), the displacement amplitude of i-th air leakage B_i can be obtained, and the pressure amplitude of the J-th acoustic mode F_J $(J = 1, 2, \ldots, N_f)$ can be calculated from the following equation (see Appendix A).

$$(\bar{k}^2 - \mathrm{j}\zeta\bar{k}\bar{k}_J - \bar{k}_J^2)\Lambda_J F_J + \frac{\rho_0\omega^2\pi^2}{4}\left(\sum_{i=1}^{N_l} \frac{\alpha_{iJ}\sum_{I=1}^{N_f} F_I\beta_{iI}}{-m\omega^2 + \mathrm{j}\omega Q_i}\right) = \frac{\rho_0\omega^2\pi^2}{4}\left(\sum_{i=1}^{N_l} \frac{\alpha_{iJ} f_e}{-m\omega^2 + \mathrm{j}\omega Q_i}\right), \tag{18}$$

The sound pressure in the frequency domain within the enclosure can then be obtained by substituting F_J into Eq. (3).

In this study, all air leakages are assumed to be square, so the variable representing the size of the i-th air leakage becomes $L_i' = L_{y_i}' = L_{z_i}'$. In the proposed methodology, the air leakage locations (y_i and z_i) and the corresponding sizes (L_i') are considered to be uncertain parameters in the identification process. As the damping ratio is usually uncertain and difficult to identify when compared to other model parameters, the damping ratio (ζ) is also treated as an uncertain parameter in the identification process. The uncertain parameter vector for a rectangular enclosure with k square air leakages is thus

$$\boldsymbol{\theta}_k = \{\zeta, y_1, y_2, \ldots, y_k, z_1, z_2, \ldots, z_k, L_1', L_2', \ldots, L_k'\}^{\mathrm{T}}. \tag{19}$$

The total number of uncertain parameters is $N_k = 3k + 1$.

2.2. Identification of the number of leakages and the corresponding locations and sizes

We now consider the general case of an enclosure with k air leakages on the side wall, with $x = L_x$ (see Fig. 1). The model class to be considered is M_k, for $k = 1, 2, \ldots, N_M$, where N_M is the maximum number of air leakages to be considered in the system identification process. From Eq. (19), $\boldsymbol{\theta}_k \in S(\boldsymbol{\theta}_k) \subset R^{N_k}$ is the vector of uncertain model parameters, such as the leakage locations and sizes, to be identified in accordance with the Bayesian statistical framework, where N_k is the dimension of $\boldsymbol{\theta}_k$. By relying on Bayes' theorem, the posterior (or updated) PDF $p(\boldsymbol{\theta}_k|D, M_k)$ for a given set of measurements D and model classes M_k, can be expressed as

$$p(\boldsymbol{\theta}_k|D, M_k) = c_k p(\boldsymbol{\theta}_k|M_k) p(D|\boldsymbol{\theta}_k, M_k), \tag{20}$$

where c_k is a normalizing constant such that the integration of $p(\boldsymbol{\theta}_k|D, M_k)$ over the domain is equal to unity, and $p(\boldsymbol{\theta}_k|M_k) = \pi(\boldsymbol{\theta}_k)$ is the prior PDF of the set of uncertain model parameters $\boldsymbol{\theta}_k$, which allows the judgment about the relative plausibility of the values of the uncertain parameters to be incorporated. A uniform prior PDF, such that the posterior PDF depends solely on the data, is employed in this study; $p(D|\boldsymbol{\theta}_k, M_k)$ is the likelihood of the data given $\boldsymbol{\theta}_k$ of model class M_k. Under the assumption of independent Gaussian prediction errors, it is given by

$$p(D|\boldsymbol{\theta}_k, M_k) = \frac{1}{\left(\sqrt{2\pi}\sigma_k\right)^{N_D}} \exp\left[-\frac{N_D}{2\sigma_k^2} J(\boldsymbol{\theta}_k|D, M_k)\right], \tag{21}$$

where σ_k is the optimal standard deviation of the target error; $N_D = NN_O$ is the total number of measured data points; N is the total number of frequency steps considered in the system identification process; and N_O is the number of measurement stations. The function $J(\boldsymbol{\theta}_k|D, M_k)$ in Eq. (21) is the contribution of the measured data, and is given [12] by

$$J(\boldsymbol{\theta}_k|D, M_k) = \frac{1}{N_D}\sum_{n=1}^{N_O} \|\hat{f}^{(N_f)}(\mathbf{r}_n) - f^{(N_f)}(\mathbf{r}_n; \boldsymbol{\theta}_k, M_k)\|^2, \tag{22}$$

where $f^{(N_f)}(\mathbf{r}_n;\boldsymbol{\theta}_k, M_k)$ is the vector of the calculated interior sound pressure at the n-th measurement station for a given model $\boldsymbol{\theta}_k$ in M_k; $\mathbf{r}_n$ is the position vector of the n-th measurement station; $\hat{f}^{(N_f)}(\mathbf{r}_n)$ is the vector of measured interior sound pressure at the n-th measurement station, both $f^{(N_f)}(\mathbf{r}_n;\boldsymbol{\theta}_k, M_k)$ and $\hat{f}^{(N_f)}(\mathbf{r}_n)$ are of dimensions N by 1; and $\|.\|$ denotes the Euclidean norm of a vector. A smaller value of $J(\boldsymbol{\theta}_k|D, M_k)$ in Eq. (22) implies a better fit to the measurement by the corresponding model $\boldsymbol{\theta}_k$. The "optimal" (or "best") model $\hat{\boldsymbol{\theta}}_k$ in a given model class M_k for a given set of data D, can be identified by maximizing the posterior PDF $p(\boldsymbol{\theta}_k|D, M_k)$, as in Eq. (20). When a uniform prior PDF (non-informative prior) is chosen in Eq. (20), this is equivalent to maximizing the likelihood of $p(D|\boldsymbol{\theta}_k, M_k)$ in Eq. (21) or minimizing the $J(\boldsymbol{\theta}_k|D, M_k)$ function in Eq. (22).

To select the "optimal" class of models from the N_M model classes, the proposed methodology allows the calculation of the probability of the model class conditional on a set of measured interior sound pressure D. Based on the Bayes' theorem,

$$P(M_k|D) = \frac{P(M_K)P(D|M_k)}{\sum_{i=1}^{N_m} P(M_i)P(D|M_i)} \quad \text{for } k = 1,\ldots,N_M, \tag{23}$$

where $1/\sum_{i=1}^{N_m} P(M_i)P(D|M_i)$ is a normalizing constant. As the number of leakages is not known, the prior probability $P(M_k)$ is taken as $1/N_M$. The most important term in Eq. (23) is the probability of getting the set of measurement D conditional on the class of models M_k. This conditional probability is called the evidence of the model class M_k. For a globally identifiable case [12,15], the evidence of M_k can be calculated based on the asymptotic approximation [16–18]

$$P(D|M_k) \approx p(D|\hat{\boldsymbol{\theta}}_k, M_k)(2\pi)^{N_k/2} p(\hat{\boldsymbol{\theta}}_k|M_k)|\mathbf{H}_k(\hat{\boldsymbol{\theta}}_k)|^{-(1/2)} \quad \text{for } k = 1,\ldots,N_M \tag{24}$$

where $\hat{\boldsymbol{\theta}}_k$ denotes the optimal model in the model class M_k. N_k is the number of uncertain model parameters in $\hat{\boldsymbol{\theta}}_k$, and $\mathbf{H}_k(\hat{\boldsymbol{\theta}}_k)$ is the Hessian of the function $g(\boldsymbol{\theta}_k)$ evaluated at the optimal model $\hat{\boldsymbol{\theta}}_k$, where $g(\boldsymbol{\theta}_k)$ is given by

$$g(\boldsymbol{\theta}_k) = -\ln[p(\boldsymbol{\theta}_k|M_k)p(D|\boldsymbol{\theta}_k, M_k)]. \tag{25}$$

When the value of N_D increases, the determinant of the Hessian $\mathbf{H}_k(\hat{\boldsymbol{\theta}}_k)$ can be approximated as

$$|\mathbf{H}_k(\hat{\boldsymbol{\theta}}_k)| \approx N_D^{N_k}|\mathbf{Q}(\hat{\boldsymbol{\theta}}_k)|, \tag{26}$$

where $\mathbf{Q}(\hat{\boldsymbol{\theta}}_k)$ is the Fisher information matrix [19]. By substituting Eq. (26) into Eq. (24), the logarithm of the evidence of M_k can be expressed as

$$\ln P(D|M_k) \approx \ln p(D|\hat{\boldsymbol{\theta}}_k, M_k) + \frac{N_k}{2}(\ln 2\pi - \ln N_D) + \ln p(\hat{\boldsymbol{\theta}}_k|M_k) - \frac{1}{2}\ln|\mathbf{Q}_k(\hat{\boldsymbol{\theta}}_k)|. \tag{27}$$

Asymptotically, the prior distribution of uncertain parameters $p(\hat{\boldsymbol{\theta}}_k|M_k)$ can be approximated by a multivariate Gaussian distribution with means $\hat{\boldsymbol{\theta}}_k$ and covariance $\mathbf{Q}^{-1}(\hat{\boldsymbol{\theta}}_k)$. As a result, the BIC [13] of the model class M_k can be obtained from Eq. (27).

$$BIC_k = \ln P(D|M_k) \approx \ln p(D|\hat{\boldsymbol{\theta}}_k, M_k) - \frac{N_k}{2}\ln N_D. \tag{28}$$

The BIC_k in Eq. (28) consists of two factors. The first factor, $\ln p(D|\hat{\boldsymbol{\theta}}_k, M_k)$, is the logarithm of the likelihood. This will be larger for model classes that correspond more closely with the interior sound pressure D. This favours model classes with more parameters (model classes with higher complexity). The second factor $(N_k/2)\ln N_D$, is a penalty for the complexity of the model class. The penalty increases with the number of data points N_D and the number of uncertain parameters N_k in the class of models. Thus, it provides a penalty against parameterization. The combining effect of these two elements makes it possible to select a model class that, on one hand, is complex enough to accurately accommodate the measurement D, and, on the other hand, is simple enough to prevent excessive "fitting" of the noise portion of the measured data.

A computationally efficient algorithm is developed for identifying the number of leakages in the enclosure without assuming the value of N_M. The algorithm consists of a series of iteration steps, as shown in Fig. 2, and begins by initializing the iteration counter k, which represents the number of leakages at the current iteration step. When $k = 0$, the algorithm checks whether the measured sound pressure data $\hat{f}(\mathbf{r}_n)$, for $n = 1$ to N_O,

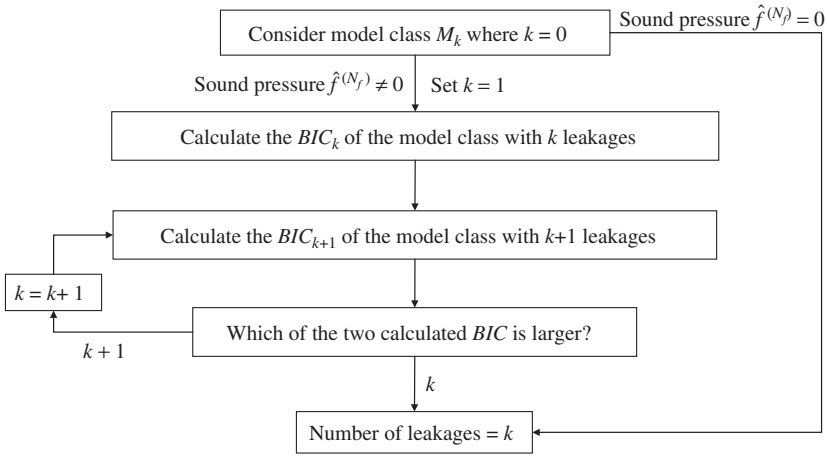

Fig. 2. The proposed algorithm for identifying the number of air leakages.

in Eq. (22) is a null vector. When there is no leakage, the measured interior sound pressure in all stations must be zero. If this is the case, then the algorithm stops, as there is no leakage. Otherwise, the algorithm will increase the k counter by 1 ($k = 1$) and calculate the values of BIC_k and BIC_{k+1}. If the value of BIC_k is larger than that of BIC_{k+1}, then the algorithm stops, and the number of leakages is equal to the value of the counter k. Otherwise, the algorithm will start the next iteration by increasing the counter k by 1 ($k = k+1$), then it will compute and compare the values of BIC_k and BIC_{k+1} again. The iteration will continue until the value of BIC_k is larger than that of BIC_{k+1} (see Fig. 2).

2.3. Calculation of the posterior probability density function of the model parameters

After identifying the number of air leakages, for example N_l, the next step of the proposed methodology is to calculate the posterior PDF $p(\boldsymbol{\theta}_{N_l}|D, M_{N_l})$ of the set of uncertain parameters $\boldsymbol{\theta}_{N_l}$ in the model class M_{N_l} for a given set of data D. For identifiable cases, the posterior PDF $p(\boldsymbol{\theta}_{N_l}|D, M_{N_l})$ can be approximated as a weighted sum of Gaussian distributions centered at the N_q optimal models [12]:

$$P(\boldsymbol{\theta}_{N_l}|D, M_{N_l}) \approx \sum_{q=1}^{N_q} w_q \mathbf{N}(\hat{\boldsymbol{\theta}}_{N_l}^{(q)}, A_N^{-1}(\hat{\boldsymbol{\theta}}_{N_l}^{(q)})), \tag{29}$$

where $\mathbf{N}(\boldsymbol{\mu}, \boldsymbol{\Sigma})$ denotes a multivariate Gaussian distribution with mean $\boldsymbol{\mu}$ and covariance matrix $\boldsymbol{\Sigma}$. The covariance matrix $A_N^{-1}(\hat{\boldsymbol{\theta}}_{N_l}^{(q)})$ is the Hessian of the function $N_K \ln J(\boldsymbol{\theta}_{N_l}|D, M_{N_l})$, where $N_K = (NN_O - 1)/2$ is evaluated at $\hat{\boldsymbol{\theta}}_{N_l}^{(q)}$, where $J(\boldsymbol{\theta}_{N_l}|D, M_{N_l})$ is given by Eq. (22) by replacing the variable k with the identified leakage number N_l. The weighting coefficients in Eq. (29) are given by

$$w_q = \frac{w'_q}{\sum_{q=1}^{N_q} w'_q} \quad \text{where } w'_q = \pi(\hat{\boldsymbol{\theta}}_{N_l}^{(q)})|A_N(\hat{\boldsymbol{\theta}}_{N_l}^{(q)})|^{-(1/2)}, \tag{30}$$

and where $\pi(\hat{\boldsymbol{\theta}}_{N_l}^{(q)})$ is the prior PDF $p(\boldsymbol{\theta}_{N_l}|M_{N_l})$ of the set of uncertain model parameters $\boldsymbol{\theta}_{N_l}$ evaluated at $\hat{\boldsymbol{\theta}}_{N_l}^{(q)}$. Instead of pinpointing the leakage locations and sizes, the proposed methodology aims to calculate the posterior PDF of the parameters $\boldsymbol{\theta}_{N_l}$. As a result, the level of confidence in the results of the identification can be quantified.

3. Numerical case study

A rectangular enclosure with dimensions $L_x = 6\,\text{m}$, $L_y = 4\,\text{m}$ and $L_z = 3\,\text{m}$, subjected to a uniform random sound pressure, is used as a verification example (see Fig. 1), and the dimensions and material properties of the

enclosure are summarized in Table 1. Three interior sound pressure measurement stations are located at ($x = 1.05$ m, $y = 2.15$ m, $z = 1.15$ m), ($x = 3.15$ m, $y = 3.30$ m, $z = 2.15$ m) and ($x = 4.45$ m, $y = 0.95$ m, $z = 0.75$ m). One external sound measurement is used for the identification process. For cases that consider the effect of modeling error, the measured and modeled interior sound pressures are simulated by the lowest 20 and 18 acoustic modes (N_J), respectively. The frequency range of the external sound pressure is from 20 to 120 Hz with 1 Hz frequency step. Measurement noise is considered by adding a 5% white noise to the calculated interior sound pressures.

In this paper, six cases (Cases A–F) are considered to verify and demonstrate the proposed system identification methodology. A summary of all cases is given in Table 2. Case A considers a single air leakage (at $y_1 = 0.92$ m and $z_1 = 1.65$ m with size $L_1' = 0.3$ m) without considering the effect of modeling error. Both of the measured and modeled interior sound pressures are generated by using the lowest 20 acoustic modes. Case B is the same as Case A, except that it considers the effect of modeling error. Case C is the same as Case B, except that the measurement noise in Case C is 15% (10% higher than that in Case B). Cases A and B can thus be used to study the effect of modeling error, whereas Cases B and C can be used to study the effect of measurement noise. Cases D and E consider two and three air leakages, respectively. The locations and sizes of these are ($y_1 = 2.42$ m, $z_1 = 0.75$ m, $L_1' = 0.25$ m) and ($y_2 = 0.92$ m, $z_2 = 1.65$ m, $L_2' = 0.3$ m) for Case D and ($y_1 = 2.42$ m, $z_1 = 0.75$ m, $L_1' = 0.25$ m), ($y_2 = 0.92$ m, $z_2 = 1.65$ m, $L_1' = 0.3$ m) and ($y_3 = 2.55$ m, $z_3 = 1.95$ m,

Table 1
Dimensional and material properties of the enclosure..

Property	Value
Thickness of wall (h)	0.1 m
Damping ratio of wall (ζ)	0.01
Sound speed (C)	343 m/s
Air density (ρ_0)	1.21 Kg/m^3

Table 2
Summary of all cases in the numerical case studies..

Case	No. of leakages	Leakage locations and sizes (m)			No. of measurement stations	Noise (%)	Modelling error
		y Location	z Location	Size			
A	1	$y_1 = 0.92$	$z_1 = 1.65$	$L_1' = 0.30$	3	5	N
B	1	$y_1 = 0.92$	$z_1 = 1.65$	$L_1' = 0.30$	3	5	Y
C	1	$y_1 = 0.92$	$z_1 = 1.65$	$L_1' = 0.30$	3	15	Y
D	2	$y_1 = 2.42$ $y_2 = 0.92$	$z_1 = 0.75$ $z_2 = 1.65$	$L_1' = 0.25$ $L_2' = 0.30$	3	5	Y
E	3	$y_1 = 2.42$ $y_2 = 0.92$ $y_3 = 2.55$	$z_1 = 0.75$ $z_2 = 1.65$ $z_3 = 1.95$	$L_1' = 0.25$ $L_2' = 0.30$ $L_3' = 0.20$	3	5	Y
F	3	$y_1 = 2.42$ $y_2 = 0.92$ $y_3 = 2.55$	$z_1 = 0.75$ $z_2 = 1.65$ $z_3 = 1.95$	$L_1' = 0.25$ $L_2' = 0.30$ $L_3' = 0.20$	2	5	Y

$L_3' = 0.2\,\text{m}$) for Case E. Cases B, D and E are employed to demonstrate the proposed methodology in identifying the enclosure with different numbers of air leakages. Case F is the same as Case E, except that the former uses only two measurement stations, which are located at ($x = 3.15\,\text{m}$, $y = 3.32\,\text{m}$, $z = 2.15\,\text{m}$) and ($x = 4.45\,\text{m}$, $y = 0.95\,\text{m}$, $z = 0.75\,\text{m}$). The effect of the number of measurement stations can thus be studied by comparing the results in Cases E and F.

3.1. Effects of the modeling error

As the modeling error is only introduced in Case B, its effects on the results of system identification can be studied by comparing the results from Cases A and B.

The proposed methodology begins by checking the measured interior sound pressures. If the measured interior sound pressure vector is not null, then there must be at least one leakage in the enclosure. The next step is to calculate the relative BIC_k (the values of BIC are normalized such that the maximum is equal to unity for easy comparison) of the model classes M_1 and M_2, which are the model classes of enclosures with one and two air leakages, respectively. The calculated results are summarized in Tables 3 and 4. It is clear from the tables that the relative BIC_1 (1 for both Cases A and B) is larger than the relative BIC_2 (3.07×10^{-4} for Case A and 9.03×10^{-4} for Case B), and therefore, it can be concluded that there is only one air leakage in the enclosure. Use of the proposed methodology allows for the successful identification of the true number of air leakages ($N_l = 1$) in both cases. Tables 3 and 4 also show the logarithms of the likelihood factor and penalty. The results show that the logarithm of likelihood and penalty are larger for more complex model classes. If the optimal model class is selected based solely on the logarithm of the likelihood factor, the most complex model class will always be chosen. It is shown in the table that the likelihood factor of the optimal model class in Case A is larger than that of the optimal model class in Case B. This is because the match between the modeled and measured interior sound pressure in Case B is affected by the modeling error.

The optimal model $\hat{\boldsymbol{\theta}}_1$ and the updated PDF of the set of model parameters $\boldsymbol{\theta}_1$ can then be calculated using the proposed methodology. The normalized marginal PDF of the air leakage location (y_1 and z_1) for both Cases A and B are plotted in Figs. 3 and 4, respectively. First of all, there is only one peak in both figures, which shows that there is only one optimal model within the domain of interest. Second, the PDF value in both figures drops significantly when one moves away from the optimal model in any direction. This is a typical characteristic of an identifiable case [20–23]. Both figures are in the same scale for comparison. It is clear that the drop in PDF value in Case A (Fig. 3) occurs much more quickly than that in Case B (Fig. 4). This is due to the fact that the uncertainties associated with the identification results in Case B (with modeling error) are higher than those associated with the identification results in Case A (without the modeling error). Figs. 5–10 show the marginal cumulative distributions of the optimal air leakage locations and sizes (y_1, z_1 and L_1') for Cases A and B. These figures provide detailed information about the uncertainties associated with the identified results. When Figs. 5–7 are compared to Figs. 8–10, respectively, it may be concluded again that the

Table 3
Model class selection results of Case A..

Class of models	Relative BIC_k	BIC_k	Logarithm of the likelihood factor	Logarithm of the penalty
M_1	1	2021.06	2032.49	−11.43
M_2	3.07×10^{-4}	2012.97	2032.97	−20.00

Table 4
Model class selection results of Case B..

Class of models	Relative BIC_k	BIC_k	Logarithm of the likelihood factor	Logarithm of the penalty
M_1	1	1628.36	1639.79	−11.43
M_2	9.03×10^{-4}	1621.35	1641.35	−20.00

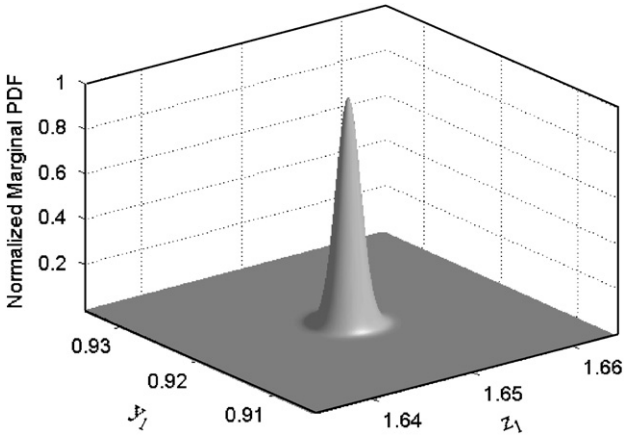

Fig. 3. Normalized marginal PDF of the air leakage location (y_1 and z_1) in Case A.

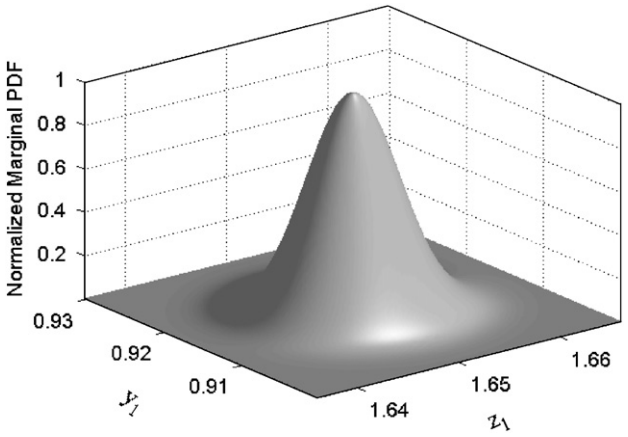

Fig. 4. Normalized marginal PDF of the air leakage location (y_1 and z_1) in Case B.

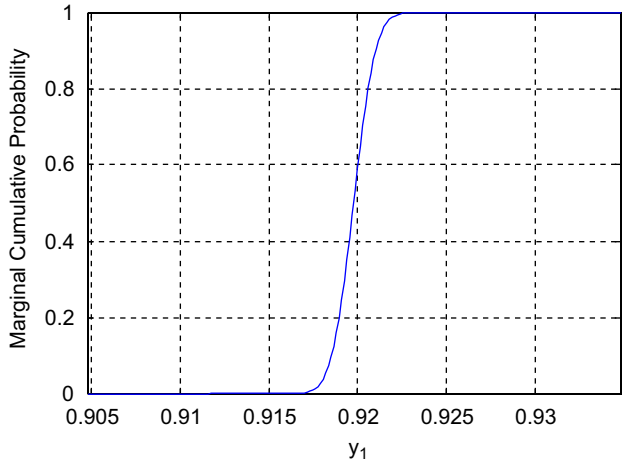

Fig. 5. Marginal cumulative distribution of the air leakage location (y_1) in Case A.

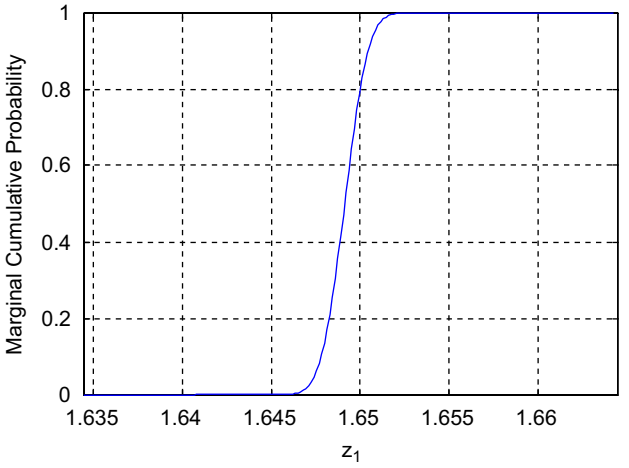

Fig. 6. Marginal cumulative distribution of the air leakage location (z_1) in Case A.

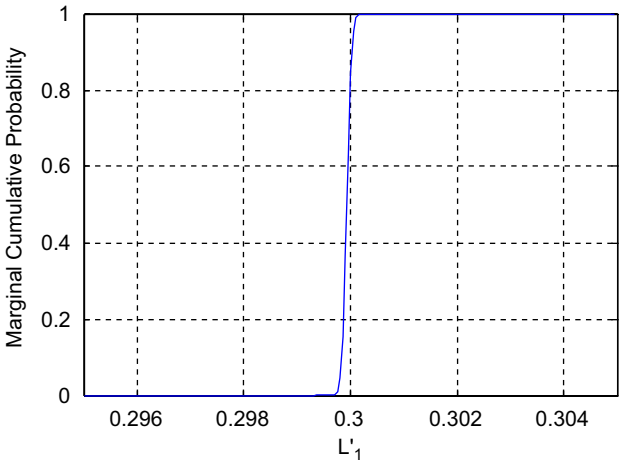

Fig. 7. Marginal cumulative distribution of the air leakage size (L_1') in Case A.

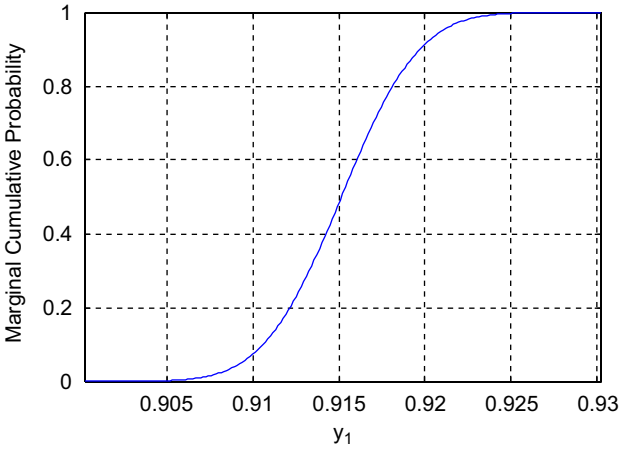

Fig. 8. Marginal cumulative distribution of the air leakage location (y_1) in Case B.

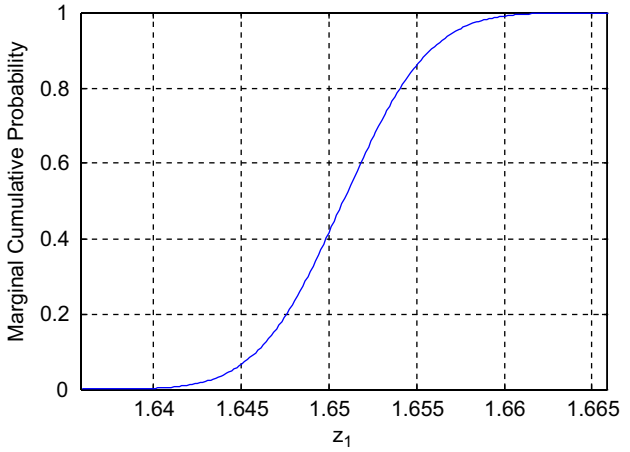

Fig. 9. Marginal cumulative distribution of the air leakage location (z_1) in Case B.

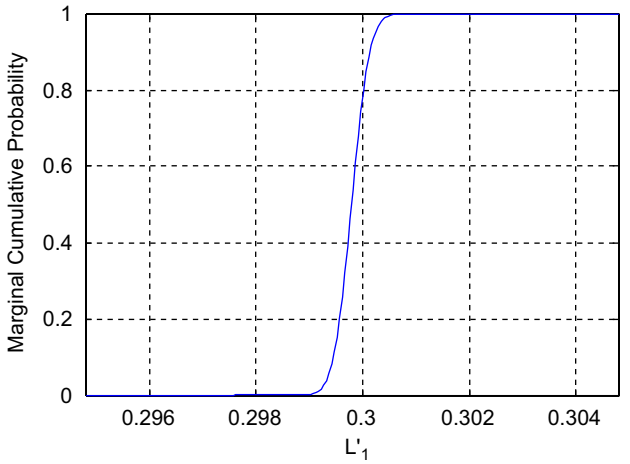

Fig. 10. Marginal cumulative distribution of the air leakage size (L_1') in Case B.

uncertainties associated with the identified results in Case A are less that those associated with the identified results in Case B.

The uncertainties can also be quantified by the coefficients of variation (COVs) for all uncertain model parameters, which are calculated based on the updated PDFs. The calculated COV values are summarized together with the optimal parameters in Table 9. From the second to the fourth rows of the table, the optimal air leakage location and the corresponding size are $y_1 = 0.9198$ m, $z_1 = 1.6495$ m and $L_1^{'} = 0.3000$ m for Case A, with COV values 0.11%, 0.06% and 0.03%, respectively. For Case B, the results are $y_1 = 0.9152$ m, $z_1 = 1.6509$ m and $L_1' = 0.2998$ m, with COV values 0.39%, 0.23% and 0.09%, respectively. The identified damping ratio is shown in the fifth row of the table, and the results are $\zeta = 0.01$ for both cases, with COV values 0.21% and 0.77%. The results are very encouraging, as all of the identified results are very close to the true values. Furthermore, the values of the COV clearly show that modeling error increases the uncertainties associated with the results of system identification. This conclusion is aligned with the observation from the normalized marginal PDF (Figs. 3 and 4) and marginal cumulative distribution plots (Figs. 5–10).

3.2. *Effects of the measurement noise*

Case C is the same as Case B, except that the measurement noise in Case C is 15% (that is, 10% higher than that in Case B). Because the measured interior sound pressure is not zero, there is at least one leakage in the

enclosure in Case C. According to the proposed methodology, the next step is to calculate the BIC values for model classes M_1 and M_2. Table 5 clearly shows that the relative BIC_1 (1) is larger than BIC_2 (5.16×10^{-4}). Therefore, it can be concluded that there is only one leakage in the enclosure in Case C. Using the proposed methodology, we successfully identified the true number of air leakages ($N_l = 1$). By comparing the likelihood factors of the optimal model class in Cases B and C, it can be concluded that the uncertainties of the identified results in Case C are higher due to the increase in measurement noise.

Table 9 shows the optimal air leakage location and size, together with the damping ratio. All of the identified results are very close to the true values. It is clear that the COV values in Case C are larger than those in Case B. Because Case C has a higher measurement noise than Case B, the increase in the uncertainties associated with the identified results is expected.

3.3. Effects of the number of air leakages

Cases D and E consider the same measurement noise and modeling error, but the numbers of leakages are different. Case D has two air leakages, whereas Case E has three. When compared to Case B, Case D has an additional small air leakage ($L_2' = 0.25$). When compared to Case E, Case D has one less air leakage with size $L_2' = 0.2$. Because the measured interior sound pressure in both cases is not zero, there is at least one leakage in each case. The relative BIC_k for M_1 and M_2 is then calculated for both examples. Tables 6 and 7 show the calculated relative BIC_k values. From Table 6 (Case D), it is clear that the relative BIC_2 (1) is larger than BIC_1 (1.47×10^{-273}). According to the algorithm, there must be at least two leakages in Case D. The algorithm continues to calculate the relative BIC_3, which is equal to 1.88×10^{-4} (see Table 6). Hence, it can be concluded that there are only two air leakages ($N_l = 2$) in Case D. Similarly, Table 7 shows the relative BIC_k of model class M_1 (8.78×10^{-345}), M_2 (3.27×10^{-98}), M_3 (1) and M_4 (2.10×10^{-4}) in Case E. It is clear from the table that the relative BIC_3 is the largest. Again, the proposed methodology accurately identifies the true number of leakages.

The optimal model parameters, together with the corresponding COV values in Cases D and E, are summarized in Table 9. It is clear from the table that all of the identified model parameters are very close to the simulated values. Table 9 also shows that the COV values in Case D (two leakages) are in general larger than those in Case B (one leakage). Similarly, the COV values in Case E (three leakages) are in general greater than those in Case D (two leakages). These results reveal that the uncertainties of system identification will increase when the number of leakages increases. This can be explained by the fact that the number of uncertain model parameters increases when the number of leakages increases. For a given set of measurements (constant amount of information), the larger the number of uncertain parameters, the higher the associated uncertainties will be [24].

3.4. Effects of the number of measurement stations

Case F is the same as Case E, except that there are only two measurement stations in Case F. The calculated values of the relative BIC_k are summarized in Table 8, which shows that the relative BIC_k increases from M_1 to M_3 (from 9.95×10^{-208} to 1) and decreases from M_3 to M_4 (from 1 to 7.17×10^{-4}), demonstrating that the correct number of air leakages in Case F is three. The optimal air leakage locations and the corresponding optimal sizes, together with the optimal damping ratio, are summarized in Table 9. All of the identified results are close to the true values.

Table 5
Model class selection results of Case C..

Class of models	Relative BIC_k	BIC_k	Logarithm of the likelihood factor	Logarithm of the penalty
M_1	1	1567.82	1579.25	−11.43
M_2	5.16×10^{-4}	1560.25	1580.25	−20.00

Table 6
Model class selection results of Case D..

Class of models	Relative BIC_k	BIC_k	Logarithm of the likelihood factor	Logarithm of the penalty
M_1	1.47×10^{-273}	1019.26	1030.69	−11.43
M_2	1	1647.47	1667.47	−20.00
M_3	1.88×10^{-4}	1638.91	1667.48	−28.57

Table 7
Model class selection results of Case E..

Class of models	Relative BIC_k	BIC_k	Logarithm of the likelihood factor	Logarithm of the penalty
M_1	8.78×10^{-345}	901.39	912.82	−11.43
M_2	3.27×10^{-98}	1469.14	1489.14	−20.00
M_3	1	1693.61	1722.18	−28.57
M_4	2.10×10^{-4}	1685.14	1722.28	−37.14

Table 8
Model class selection results of Case F..

Class of models	Relative BIC_k	BIC_k	Logarithm of the likelihood factor	Logarithm of the penalty
M_1	9.95×10^{-208}	651.53	662.15	−10.62
M_2	3.25×10^{-69}	970.47	989.04	−18.57
M_3	1	1128.17	1154.71	−26.54
M_4	7.17×10^{-4}	1120.93	1155.43	−34.50

Table 9
Optimal parameters and the corresponding COV in all cases..

Case	Leakage locations and sizes (m)			Damping ratio (COV%)
	y Location (COV%)	z Location (COV%)	Size (COV%)	
A	$y_1 = 0.9198$ (0.11)	$z_1 = 1.6495$ (0.06)	$L'_1 = 0.3000$ (0.03)	0.0100 (0.21)
B	$y_1 = 0.9152$ (0.39)	$z_1 = 1.6509$ (0.23)	$L'_1 = 0.2998$ (0.09)	0.0100 (0.77)
C	$y_1 = 0.9162$ (0.48)	$z_1 = 1.6499$ (0.29)	$L'_1 = 0.2998$ (0.11)	0.0100 (0.94)
D	$y_1 = 2.3901$ (0.42) $y_2 = 0.8957$ (1.00)	$z_1 = 0.7571$ (1.46) $z_2 = 1.6658$ (0.43)	$L'_1 = 0.2540$ (0.70) $L'_2 = 0.2964$ (0.53)	0.0101 (0.87)
E	$y_1 = 2.4416$ (0.44) $y_2 = 0.9163$ (0.81) $y_3 = 2.5156$ (0.82)	$z_1 = 0.7597$ (5.02) $z_2 = 1.6396$ (0.35) $z_3 = 1.9876$ (3.06)	$L'_1 = 0.2513$ (2.58) $L'_2 = 0.3000$ (0.43) $L'_3 = 0.1982$ (4.23)	0.0100 (1.15)
F	$y_1 = 2.4635$ (0.71) $y_2 = 0.9121$ (1.29) $y_3 = 2.4842$ (1.31)	$z_1 = 0.7489$ (5.12) $z_2 = 1.6321$ (0.56) $z_3 = 1.9966$ (3.44)	$L'_1 = 0.2492$ (2.63) $L'_2 = 0.2996$ (0.61) $L'_3 = 0.2015$ (4.34)	0.0101 (1.23)

Table 9 also shows the COV values of the identified results. It is clear from the table that the COV values in Case F are larger than those in Case E. This can be explained by the fact that the amount of information available for system identification in Case E (three measurement stations) is greater than that in Case F (two measurement stations).

4. Discussion and conclusions

In this paper, we presented a methodology for the system identification of a rectangular enclosure with an unknown number of air leakages. The locations and sizes of the air leakages, together with the damping ratio of the system, are treated as uncertain model parameters. Unlike other model-based identification techniques in the literature, the proposed methodology is applicable when the number of air leakages is not given in advance. The proposed methodology relies on the BIC to identify the number of air leakages, based on a set of measured interior sound pressure in the frequency domain. One outstanding advantage of the proposed methodology, when compared to other deterministic techniques, is that the uncertainties associated with the identification results can be quantified through the calculation of the posterior PDF of model parameters.

The numerical case studies investigate the effects of modeling error, measurement noise, the number of air leakages and the number of measurement stations in the accuracy of the identification results. The verification results show that the proposed methodology can successfully identify the simulated air leakages in the presence of measurement noise and modeling error. As expected, both the modeling error and measurement noise increase the uncertainty associated with the identified results. The case study also shows that the uncertainties of system identification will increase when the number of leakages increases. The increase in the number of measurement stations leads to a reduction in COV of the identified results. That is, the uncertainties of the identification results are reduced. This is to be expected as an additional measurement station increases the amount of information for the purpose of system identification. The series of case studies shows that the Bayesian approach provides a robust measure for quantifying uncertainty.

Although it was assumed in the derivation that the enclosure and the leakages are rectangular, it is possible to modify the formulations for other shapes of enclosures and leakages. Furthermore, all leakages are assumed on one of the side walls in the case study, the proposed methodology can easily be extended to cases in which the leakages are on any of the side walls by considering more model classes.

Acknowledgment

The work described in this paper was fully supported by a grant from the Research Grants Council of the Hong Kong Administrative Region, China (Project no. CityU 114706).

Appendix A

This appendix shows the derivation of Eq. (18). By combining Eqs. (14), (15) and (16), the air particle displacement amplitudes at the i-th air leakage B_i can be represented as

$$B_i = \frac{\pi^2}{4(-m\omega^2 + \mathrm{j}\omega Q_i)} \left(\sum_{I=1}^{N_f} F_I \beta_{iI} - f_e \right) \tag{A.1}$$

By substituting Eq. (A.1) into (12), the following relation can be obtained

$$\int_S \phi_J \frac{\partial f^{(N_f)}(\mathbf{r})}{\partial n} \mathrm{d}S = \frac{\rho_0 \omega^2 \pi^2}{4} \left[\sum_{i=1}^{N_l} \frac{\alpha_{iJ} (\sum_{I=1}^{N_f} F_I \beta_{iI} - f_e)}{-m\omega^2 + \mathrm{j}\omega Q_i} \right] \tag{A.2}$$

The result of Eq. (A.2) is then substituted into Eq. (8) and omitting the second term at the right-hand side of Eq. (8) which is related to the point sound source, the following expression can then be derived

$$(\bar{k}^2 - \mathrm{j}\zeta \bar{k} \bar{k}_J - \bar{k}_J^2) \Lambda_J F_J = -\frac{\rho_0 \omega^2 \pi^2}{4} \left[\sum_{i=1}^{N_l} \frac{\alpha_{iJ} (\sum_{I=1}^{N_f} F_I \beta_{iI} - f_e)}{-m\omega^2 + \mathrm{j}\omega Q_i} \right] \tag{A.3}$$

The Eq. (18) is finally obtained by rearranging Eq. (A.3).

References

[1] A.J. Pretlove, Free vibration of a rectangular panel backed by a closed rectangular cavity, *Journal of Sound and vibration* 2 (3) (1965) 197–209.

[2] A.J. Pretlove, Forced vibration of a rectangular panel backed by a closed rectangular cavity, *Journal of Sound and vibration* 3 (3) (1966) 252–261.

[3] S. Narayanan, R.L. Shanbhag, Sound transmission through elastically supported sandwich panels into a rectangular enclosure, *Journal of Sound and Vibration* 77 (2) (1981) 251–270.

[4] D.J. Oldham, S.N. Hillarby, The acoustical performance of small close fitting enclosure—part 1: theoretical models, *Journal of Sound and Vibration* 150 (2) (1991) 261–281.

[5] J. Pan, S.J. Elliott, K.H. Baek, Analysis of low frequency acoustic response in a damped rectangular enclosure, *Journal of Sound and Vibration* 223 (4) (1999) 543–566.

[6] D.J. Oldham, S.N. Hillarby, The acoustical performance of small close fitting enclosure—part 2: experimental investigation, *Journal of Sound and Vibration* 150 (2) (1991) 283–300.

[7] T. McKelvey, H. Akcay, L. Ljung, Subspace-based multivariable system identification from frequency response data, *IEEE Transactions on Automatic Control* 41 (7) (1996) 960–979.

[8] J.K. Henry, R.L. Clark, Active control of sound transmission through a curved panel into a cylindrical enclosure, *Journal of Sound and Vibration* 249 (2) (2002) 325–349.

[9] B. Fang, A.G. Kelkar, S.M. Hoshi, H.R. Pota, Modelling, system identification, and control of acoustic-structure dynamics in 3-D enclosures, *Control Engineering Practice* 12 (2004) 989–1004.

[10] Y.Y. Lee, A.Y.T. Leung, H.F. Lam, H.Y. Sun, Reconstruction of the interior sound pressure of a room using the probabilistic approach, *Journal of Sound and Vibration* 298 (2006) 877–891.

[11] J. Lardies, Identification of a dynamical model for an acoustic enclosure using the wavelet transform, *Applied Acoustics* 68 (2007) 473–490.

[12] J.L. Beck, L.S. Katafygiotis, Updating models and their uncertainties I: Bayesian statistical framework, *Journal of Engineering Mechanics, ASCE* 124 (4) (1998) 455–461.

[13] G. Schwarz, Estimating the dimension of a model, *Annals of Statistics* 6 (2) (1978) 461–464.

[14] L.E. Kinsler, A.R. Frey, A.B. Coppens, J.V. Sander, *Fundamentals of Acoustics*, fourth ed., Wiley, New York, 2000.

[15] L.S. Katafygiotis, J.L. Beck, Updating models and their uncertainties II: model identifiability, *Journal of Engineering Mechanics, ASCE* 124 (4) (1998) 463–467.

[16] C. Papadimitriou, J.L. Beck, L.S. Katafygiotis, Asymptotic expansions for reliability and moments of uncertain systems, *Journal of Engineering Mechanics, ASCE* 123 (12) (1997) 1219–1229.

[17] J.L. Beck, K.V. Yuen, Model selection using response measurement: A Bayesian probabilistic approach, *Journal of Engineering Mechanics, ASCE* 130 (2) (2004) 192–203.

[18] H.F. Lam, K.V. Yuen, J.L. Beck, Structural health monitoring via measured Ritz vectors utilizing artificial neural networks, *Computer-Aided Civil and Infrastructure Engineering* 21 (4) (2006) 232–241.

[19] J.J. Rissanen, Fisher information and stochastic complexity, *IEEE Transactions on Information Theory* 42 (1) (1996) 40–47.

[20] L.S. Katafygiotis, H.F. Lam, Tangential-projection algorithm for manifold representation in unidentifiable model updating problems, *Earthquake Engineering & Structural Dynamics* 31 (4) (2002) 791–812.

[21] H.F. Lam, C.T. Ng, M. Veidt, Experimental characterization of multiple cracks in a cantilever beam utilizing transient vibration data following a probabilistic approach, *Journal of Sound and Vibration* 305 (2007) 34–49.

[22] H.F. Lam, Y.Y. Lee, H.Y. Sun, G.F. Cheng, X. Guo, Application of the spatial wavelet transform and Bayesian approach to the crack detection of a partially obstructed beam, *Thin-Walled Structures* 43 (1) (2005) 1–21.

[23] H.F. Lam, C.T. Ng, A probabilistic method for the detection of obstructed cracks of beam-type structures using spatial wavelet transform, *Probabilistic Engineering Mechanics* 23 (2–3) (2008) 237–245.

[24] H.F. Lam, C.T. Ng, A.Y.T. Leung, Multi-crack detection on semi-rigidly connected beams utilizing dynamic data, *Journal of Engineering Mechanics, ASCE* 134 (1) (2007) 90–99.